Robust design optimization of moment-resisting steel frame against uncertainties of surface ground properties using order statistics

AUTHOR(S):

YAMAKAWA, Makoto; OHSAKI, Makoto; WATANABE, Kana

CITATION:

YAMAKAWA, Makoto ...[et al]. Robust design optimization of moment-resisting steel frame against uncertainties of surface ground properties using order statistics. Japan-China Workshop on Analysis and Optimization of Large-scale Structures 2018: 23-31: A13.

ISSUE DATE:

2018-05-14

URL:

http://hdl.handle.net/2433/231246

Robust design optimization of moment-resisting steel frame against uncertainties of surface ground properties using order statistics

Makoto YAMAKAWA[1*], Makoto OHSAKI[2], Kana WATANABE[3],
[1*] Department of Architecture, Tokyo University of Science

6-3-1 Niijuku, Katsushika-ku, Tokyo 125-8585, Japan
myamakawa@rs.tus.ac.jp

[2] Department of Architecture and Architectural Engineering, Kyoto University
[3] Department of Architecture, Tokyo Denki University

Keywords: robust design; uncertainty; order statistics; amplification of surface ground motion

1. Introduction

For earthquake-resistant design of structures, we should appropriately consider the uncertainties in seismic loads. Without taking uncertainties of the seismic loads into consideration, severe damage might occur in the structures [1]-[5]. Robust design is known as an effective design method to cope with such uncertainties. Uncertainties in ground-surface properties such as layer thickness, and mass density, shear modulus and damping ratio of soil induces complex influence on surface-ground amplification of seismic motions. That is, the uncertainties in the ground-surface properties should be appropriately considered for the safety of the structures.

The authors proposed an approximately-worst-case method based on order statistics [3],[6]. This order-statistics-based robust design optimization can cope with structural responses in time domain and incorporate the uncertainties in the surface-ground amplification of the seismic motions to the structures. In this paper, an application is shown that a moment resisting frame with braces can possess highly-robust safety by the proposed method. It is then assumed that for the design seismic motions, their amplitudes of acceleration response spectra at engineering bedrock surface are specified by a target design spectrum [7],[8]; however, their phase spectra and ground-surface properties contain uncertainties.

2. Robust design optimization with order statistics

Let us first define a robust design problem. The design variable vector is denoted by $\mathbf{x} = (x_1, \cdots, x_d)$, where d is the number of the design variables. The vector consisting of uncertain parameters is denoted by $\boldsymbol{\theta} = (\theta_1, \cdots, \theta_r) \in \Omega$, where r is the number of the uncertain parameters and Ω is a pre-specified uncertainty set. For simplicity, only the lower and upper bounds of the variables are given as constraints, which are denoted by $\overline{x}^L \le x_i \le \overline{x}^U \quad (i = 1, \cdots, d)$, where $\overline{x}^L$ is the lower bound, $\overline{x}^U$ is the upper bound. The objective function is denoted by $g = g(\mathbf{x}; \boldsymbol{\theta})$, which is structural response function

corresponding to the design variables $\mathbf{x}$ and uncertain parameters $\boldsymbol{\theta}$. Thus, a robust design problem we are interested in can be described as Problem (1):

$$\left.\begin{array}{ll} \text{find} & \mathbf{x} = \left(x_1, \cdots, x_d\right) \\ \text{that minmizes} & g\left(\mathbf{x};\boldsymbol{\theta}\right) \quad \text{for all } \boldsymbol{\theta} \in \Omega \\ \text{subject to} & \overline{x}^L \le x_i \le \overline{x}^U \left(i = 1, \cdots, d\right) \end{array}\right\} \tag{1}$$

It is difficult to directly solve Problem (1). Against this background, we presented an approximately-worst-case method based on order statistics. The response function in Problem (1) is regarded as random variable depending on $\mathbf{x}$, which is denoted by $Y(\mathbf{x}) = g(\mathbf{x};\boldsymbol{\theta})$. By random search techniques, we obtain sample set of size n, which is denoted by $\{\boldsymbol{\theta}_1, \cdots, \boldsymbol{\theta}_n\}$ and we obtain corresponding sample values denoted by $Y_1 = g(\mathbf{x};\boldsymbol{\theta}_1), \cdots, Y_n = g(\mathbf{x};\boldsymbol{\theta}_n)$. The sample values are arranged in increasing order of magnitude as $Y_{1,n} \ge \cdots \ge Y_{k,n} \ge \cdots \ge Y_{n,n}$, which are referred to as order statistics. From the theory of order statistics [9], we can find k and n for given α and γ such that

$$\Pr\left\{\Pr\left\{Y \le Y_{k,n}\right\} \ge \gamma\right\} \ge \alpha . \tag{2}$$

Eq.(2) means that at least $100\alpha\%$ that at least a proportion γ of the population is less than $Y_{k,n}$. The sample size requirements are shown in Table 1. Thus, we formulate a new robust optimization problem based on ordered statistics as

$$\left.\begin{array}{ll} \text{find} & \mathbf{x} = \left(x_1, \cdots, x_d\right) \\ \text{that minmizes} & Y_{k,n}\left(\mathbf{x}\right) \\ \text{subject to} & \overline{x}^L \le x_i \le \overline{x}^U \left(i = 1, \cdots, d\right) \end{array}\right\} \tag{3}$$

Table 1. The sample size requirements

(a) for $\alpha = \gamma = 0.9$

k	1	2	3	4	5	6	7	8	9	10
$n(k)$	22	38	52	65	78	91	104	116	128	140
k	11	12	13	14	15	16	17	18	19	20
$n(k)$	152	164	175	187	199	210	222	233	245	256

(b) for $\alpha = 0.99, \gamma = 0.9$

k	1	2	3	4	5	6	7	8	9	10
$n(k)$	44	64	81	97	113	127	142	156	170	183
k	11	12	13	14	15	16	17	18	19	20
$n(k)$	197	210	223	236	249	262	275	287	300	312

(c) for $\alpha = 0.99 = 0.99$

k	1	2	3	4	5	6	7	8	9	10
$n(k)$	459	662	838	1001	1157	1307	1453	1596	1736	1874
k	11	12	13	14	15	16	17	18	19	20
$n(k)$	2010	2144	2277	2409	2539	2669	2798	2925	3052	3179

3. Seismic motion considering uncertain properties of surface ground

In this study, design seismic motions are generated by simple superposition of sinusoidal waves [7]. Their amplitudes of acceleration response spectra at engineering bedrock surface are specified by a design target spectrum; however, their phase spectra should contain uncertainties. Furthermore, amplification of seismic motions in surface ground is taken account, incorporating uncertainties in its properties. Thus, the seismic motions to a structure should be influenced by uncertainties in the phase spectra and the surface-ground properties.

3.1. Amplitude spectrum and phase spectrum

The discretized acceleration time history waveform at the engineering bedrock surface can be denoted by

$$\mathbf{a}^B = \left(a_0^B, \cdots, a_{N_d-1}^B\right), \tag{4}$$

$$a_m^B = \sum_{k=0}^{N_d/2} A_k \cos\left(\omega_k \cdot m\Delta t + \phi_k\right), \quad \left(m = 0, \cdots, N_d - 1\right) \tag{5}$$

where N_d is the number of the time point, ω_k is the k-th angular frequency, $\mathbf{A} = (A_0, \cdots, A_{N_d-1})$ and $\boldsymbol{\phi} = (\phi_0, \cdots, \phi_{N_d-1})$ respectively denote amplitude and phase of the discrete Fourier spectrum of the seismic motion. The design acceleration response spectrum for 5% damping at the engineering bedrock surface specified by Notification 1461 of the Ministry of Land, Infrastructure and Transport (MLIT), Japan is given as

$$S_a(T) = \begin{cases} 3.2 + 30T & \text{if } T < 0.16 \text{ sec}, \\ 8 & \text{if } 0.16 \le T < 0.64 \text{ sec}, \\ 5.12/T & \text{if } 0.64 \le T \text{ sec}, \end{cases} \tag{6}$$

where $T\ (\text{sec})$ is the natural period of the building. The design seismic motions at the engineering bedrock surface are generated as follows: (i) number c of phase spectra denoted by $\boldsymbol{\phi}_1, \cdots, \boldsymbol{\phi}_c$ are given and one of them is randomly selected, which is denoted by $\boldsymbol{\phi}(\theta_1)$, where $\theta_1 \in \{1, \cdots, c\}$ is a uncertain parameter, and (ii) an amplitude spectrum denoted by $\mathbf{A}^B$ is generated by simple superposition of sinusoidal waves to fit the design acceleration response spectrum specified by Eq.(6). Thus, the acceleration time history at the engineering bedrock surface is calculated by the inverse Fourier transform of $\mathbf{A}^B$ and $\boldsymbol{\phi}$, which can be regarded as a vector-valued function denoted by $\mathbf{a}^B = \mathbf{a}^B(\theta_1) = \mathbf{a}^B(\boldsymbol{\phi}(\theta_1); \mathbf{A}^B)$.

3.2. Seismic motion considering the uncertain amplification of surface ground

Let us consider a N-layer soil model, as shown in Figure 1. Numbering of soil layers starts at the ground surface and the engineering bedrock is given by the N-th layer. The layer thickness and the shear wave velocity of the m-th soil layer are denoted by H_m and V_m, respectively. The mass density, the shear modulus and the damping ratio of the m-th layer are respectively denoted by ρ_m, G_m and h_m. Shear modulus G and damping ratio h at given shear strain G are provided by the Hardin-Drnevich model [11] denoted by

$$G/G_0 = 1/\left(1 + \gamma/\gamma_{0.5}\right), \quad h = h_{\max}\left(1 - G/G_0\right), \tag{7),(8}$$

where G_0 is the small strain shear modulus at initial loading, $h_{\max}$ is the maximum damping ratio at maximum strain and $\gamma_{0.5}$ is the reference shear strain. In Eq.(7) and Eq.(8), the reference shear strain and the maximum damping ratio are respectively given as $\gamma_{0.5} = 0.15\%$ and $h_{\max} = 15\%$.

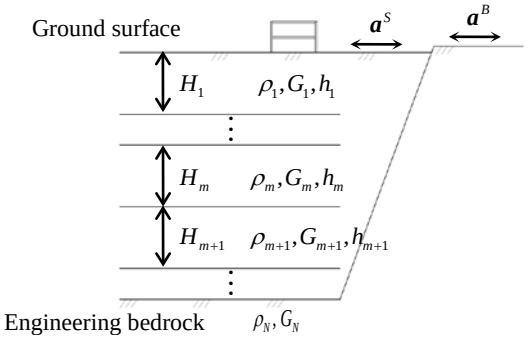

Figure 1. *N*-layer soil model

Nonlinear dependency of shear modulus and damping ratios on the strain level should be considered. We use an equivalent linear method to obtain input seismic motions to a structure [10], in which shear modulus and damping ratio are assumed to be given, and the maximum shear strain $\gamma_{\max}$ are evaluated by some linear analyses. In a linear analysis, the incident wave and the reflected wave in m-th soil layer are denoted by E_m and F_m. The recursion formulas for the amplitudes, E_{m+1} and F_{m+1} of the incident and reflected wave in the $m+1$-th layer expressed in terms of the amplitudes in the m-th layer as

$$\begin{Bmatrix} E_{m+1} \\ F_{m+1} \end{Bmatrix} = \frac{1}{2}\begin{bmatrix} (1+\alpha_m)e^{i(\omega H_m/V_m)} & (1-\alpha_m)e^{-i(\omega H_m/V_m)} \\ (1-\alpha_m)e^{i(\omega H_m/V_m)} & (1+\alpha_m)e^{-i(\omega H_m/V_m)} \end{bmatrix}\begin{Bmatrix} E_m \\ F_m \end{Bmatrix}, \tag{9}$$

where impedance ratio is denoted by $\alpha_m = \rho_m V_m / \rho_{m+1} V_{m+1}$ and shear wave velocity is denoted by $V_m = \sqrt{G_m / \rho_m}$, ω is the frequency of the harmonic displacement. The effective strain γ_{eq} is computed from the maximum strain $\gamma_{\max}$ by the linear analysis as

$$\gamma_{\text{eq}} = 0.65\gamma_{\max}, \tag{10}$$

where 0.65 in Eq.(10) is a constant of effective strain conversion. We evaluate the maximum strain $\gamma_{\max}$ by the above stated procedure and iterate it until a certain convergence criterion is satisfied. Thus, the amplitude spectrum at the surface ground denoted by $\mathbf{A}^S$ is calculated from the one at the engineering bedrock and the surface ground properties. Some ground properties are linked with uncertain parameters $\theta_2, \cdots, \theta_r$ and the amplitude spectrum at the surface ground is regarded as a vector-valued function denoted by $\mathbf{A}^S = \mathbf{A}^S(\theta_2, \cdots, \theta_r; \mathbf{A}^B)$. The acceleration time-history at the surface ground is obtained by the inverse Fourier transform of $\mathbf{A}^S$ and $\boldsymbol{\phi}$, which is denoted by $\mathbf{a}^S = \mathbf{a}^S(\boldsymbol{\theta}) = \mathbf{a}(\boldsymbol{\phi}(\theta_1), \mathbf{A}^S(\theta_2, \cdots, \theta_r; \mathbf{A}^B))$. The response of the building depending on design variable vector $\mathbf{x}$ corresponding to the seismic motion of the surface ground with uncertainty is denoted by $Y(\mathbf{x}) = g(\mathbf{x}; \boldsymbol{a}^S(\boldsymbol{\theta}))$. Thus, we link robust design optimization with amplification of seismic ground motion by uncertain surface ground properties based on order statistics expressed by Eq.(3).

4. Numerical example

4.1. Uncertain parameters

We assume a phase spectrum of a design seismic motion, layer thickness, and shear wave velocity of the surface ground have uncertainties. The number of the uncertain parameters is set to $r = 3$. We use some phase spectra of recorded seismic motions. The number of phase spectra is set to $c = 3$, the phase spectra are given by Hachinohe EW of the Tokachi-oki Earthquake in 1968, Tohoku University NS of the Miyagi-oki Earthquake in 1978 and Kobe NS of the Hyogoken-Nambu Earthquake in 1995, which are denoted by $\boldsymbol{\phi}(1), \boldsymbol{\phi}(2), \boldsymbol{\phi}(3)$, respectively. One of them is randomly selected as $\boldsymbol{\phi}(\theta_1)$ with $\theta_1 \in \{1,2,3\}$. We consider a two-layer ground model as shown in Figure 2, i.e., $N = 2$, layer thickness and shear wave velocity of the surface ground are taken as the uncertain parameters in Ω denoted by $(\theta_2, \theta_3) = (H_1, V_1)$. Let us set

$$\Omega = \left\{ (\theta_1, \theta_2, \theta_3) \mid \theta_1 \in \{1,2,3\}, 40\text{m} \le \theta_2 \le 60\text{m}, 100\,\text{m/s} \le \theta_3 \le 400\,\text{m/s} \right\}. \quad (11)$$

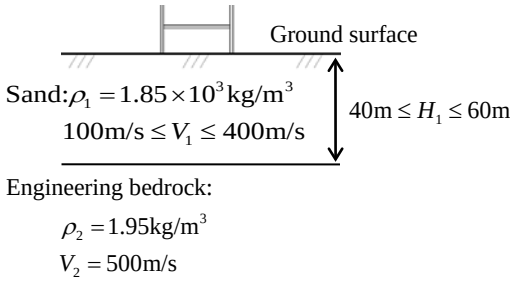

Figure 2. Two-layer ground model

4.2. Building model

Let us consider a 9-story 2-bay braced steel frame as shown in Figure 3. The beams are rigidly connected to the columns and the ends of the braces are pinned. The steel sections of beams and columns are summarized in Table 2. List of element sections H-shaped cross sections are used for the beams, and their height (mm), flange width (mm), web thickness (mm) and flange thickness (mm) are shown in Table 2. Square hollow structural sections are used for the columns, and their height (mm) and thickness (mm) are also shown in Table 2. Furthermore, we use buckling-restrained braces as the brace. The cross-sectional area of central steel material (cm^2) of each buckling-restrained brace is taken as the design variable as shown in Table 2. The number of design variable vector is set to $d = 9$. The design variable vector given upper and lower bounds are given as $\overline{x}^U = 200\text{cm}^2$, $\overline{x}^L = 0\text{cm}^2$. The steel materials of the elements are assumed to have bilinear stress strain relations, where Young's modulus is $E = 205\text{kN/mm}^2$, and the kinematic hardening ratio is $0.01E$. The yield stress is given as $\sigma_y = 325\text{N/mm}^2$ for beams and columns, $\sigma_y = 100\text{N/mm}^2$ for braces. The floor mass of $7.2 \times 10^4\text{kg}$ is distributed to the nodes of each floor. The floor diaphragm is assumed to be rigid, i.e., the horizontal displacements of the nodes on the same floor has the same value. Considering composite action of the steel beam and the concrete slab, we multiply the factor 1.5 to the flexural rigidity of each beam.

Table 2. List of element sections

Beam	
2F to 4F	H-500×250×12×25
5F to 7F	H-500×250×12×22
8F to RF	H-500×250×9×19
Column	
1S to 3S	HSS-400×25
4S to 6S	HSS-400×22
7S to 9S	HSS-400×19
Brace (Cross-sectional area of brace)	
1S to 9S	$0 \le x_i \le 200\,(i=1,\cdots,9)$

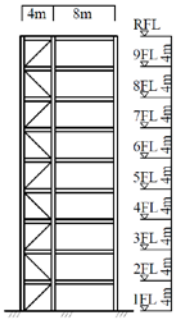

Figure 3. Steel frame

4.3. Seismic response analysis

A software framework for developing applications to simulate the performance of structural and geotechnical systems subjected to earthquakes called OpenSees [12] is used for seismic response analysis of the frame. The initial stiffness proportional damping is used with the damping ratio 0.02 for the first mode. Each beam and column is modelled by a force-based beam-column element, the section of which is divided into fibers. The flange and web of the beam are discretized into 4 and 16 fibers, respectively. The integration along the element is based on Gauss-Lobatto quadrature rule. The number of integration points is 8. The standard Newmark-β method ($\beta = 0.25,\ \gamma = 0.5$) is used for transient analysis with increment of 0.005sec. The seismic motion with duration $T_d = 120\text{sec}$ is applied.

4.4. Numerical results

We choose the maximum inter-story drift angle as the response function of this example, which is denoted by $Y(\mathbf{x}) = g(\mathbf{x};\boldsymbol{a}^S(\boldsymbol{\theta}))$. As a robust design optimization, we find $\mathbf{x}$ such that minimizes $Y_{k,n}(\mathbf{x})$ for $(k,n) = (2,38)$ corresponding to $\alpha = \gamma = 0.9$, which is referred to as Robust Optimal Solution (ROS) denoted by Eq.(3). For comparison, we also find $\mathbf{x}$ that minimizes the maximum inter-story drift angle without considering uncertain amplification of surface ground denoted by

$$\left.\begin{array}{lll} \text{find} & \mathbf{x} = (x_1, x_2, \cdots, x_d) & \\ \text{that minimize} & \max\left\{ g\left(\mathbf{x};\boldsymbol{a}^B(\theta)\right)\right\} & (\theta = 1,2,3) \\ \text{subjec to} & \overline{x}^L \le x_i \le \overline{x}^U & (i = 1,\cdots,d) \end{array}\right\}, \tag{12}$$

which is referred to as Nominal Optimal Solution (NOS). Each optimal solution is shown in Table 3. The average cross section of 1 to 3 stories of ROS is 1.3 times larger than those of NOS, and the average cross section of 7 to 9 story of ROS is half of those of NOS.

To test the validity, we apply Monte Carlo simulation to ROS and NOS with random samples of size 1000. The maximum value and the mean value, standard deviation of observed maximum inter-story drift angles of them with sample size of 1000 are summarized in Table 4. The values in 10% of the worst value are also shown in Table 4. Moreover, the value of the order statistic $Y_{2,38}(\mathbf{x})$ and the ratio of the number of samples smaller than $Y_{2,38}(\mathbf{x})$ are also summarized in Table 4. The standard deviation

in ROS decreases by 41% from the ones in NOS. The numerical result indicates the use of several tens samples enables to predict the approximately 90% worst value with 90% accuracy. Histogram of observed maximum inter-story drift angles is shown in Figure 4. Observed maximum inter-story drift angle of each story is also plotted in Figure 5. The figures indicate the variation of maximum inter-story drift angles of ROS is lower than those of NOS.

Table 3. Optimal solutions (Cross section of brace, unit: cm^2)

	x_1	x_2	x_3	x_4	x_5	x_6	x_7	x_8	x_9
ROS	150	198	145	142	108	74	60	200	25
NOS	102	150	133	102	126	94	200	200	115

Table 4. Summary of observed maximum inter-story drift angles

	Maximum (rad)	Mean (rad)	Standard deviation (rad)	Worst10 (rad)	$Y_{2,38}$ (rad)	Ratio (%)
ROS	0.023	0.014	0.0025	0.017	0.020	98
NOS	0.030	0.014	0.0042	0.021	0.027	98

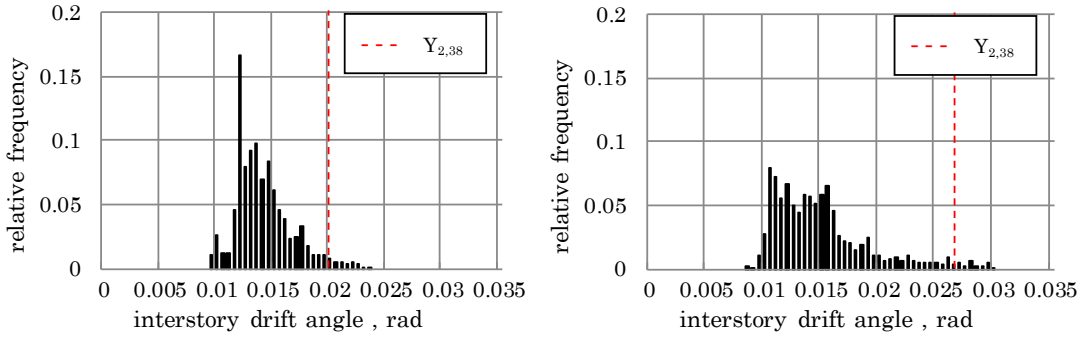

(a) Robust optimal solution (ROS) (b) Nominal optimal solution (NOS)

Figure 4. Histogram of observed maximum inter-story drift angles

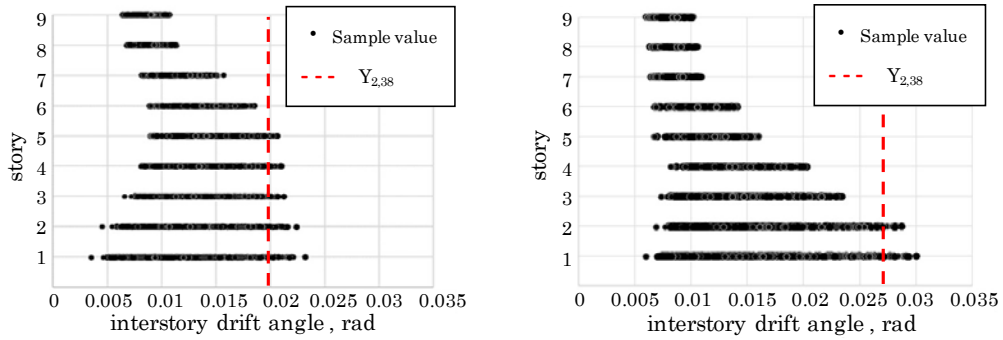

(a) Robust optimal solution (ROS) (b) Nominal optimal solution (NOS)

Figure 5 Observed maximum inter-story drift angles of story

5. Conclusions

To consider uncertainties in ground-surface properties and phase of a design seismic motion, a robust optimal design based on order statistics has been proposed. The results through a numerical example are as follows:

1. By the proposed method, we can design structures considering uncertainties in ground-surface properties and phase of a design seismic motion.
2. The robust design has smaller standard deviation of the maximum inter-story drift angle than the nominal optimal design against uniform random distribution of uncertain parameters.
3. By arranging large cross section of braces at the lower stories and small ones at the upper stories, we can obtain a robust-designed structure, considering uncertainties in the ground properties and the phase of the design seismic motion.
4. The application results indicate that several tens of samples can predict the approximately 90% worst value with 90% accuracy.

Acknowledgements

This work was supported by NSFC-JSPS China- Japan Scientific Cooperation Project.

References

[1] N. D. Lagaros and M. Papadrakakis, Robust seismic design optimization of steel structures. Structural and Multidisciplinary Optimization, 33(6): 457-469, 2007.

[2] M. V. R. Rao, A. Pownuk, S. Vandewalle amd D. Moens, Transient response of structures with uncertain structural parameters. Struct Saf, 32(6): 449-460, 2010.

[3] M. Ohsaki and M. Katsura, A random sampling approach to worst-case design of structures. Structural and Multidisciplinary Optimization, 46(1): 27-39, 2012.

[4] A. K. Kazantzi, D. Vamvatsikos and D. G. Lignos. Seismic performance of a steel moment-resisting frame subject to strength and ductility uncertainty. Eng Struct, 78, 69-77, 2014.

[5] Z. Liu, S. Atamturktur and C. H. Juang, Reliability based multi-objective robust design optimization of steel moment resisting frame considering spatial variability of connection parameters. Eng Struct, 76: 393-403, 2014.

[6] M. Yamakawa and M. Ohsaki, Worst-case design of structures using stopping rules in k-adaptive random sampling approach. In Proc. 10th World Congress on Structural and Multidisciplinary Optimization, ISSMO, Orlando, 2013.

[7] R. N. Iyengar and P. N. Rao, Generation of spectrum compatible accelerograms. Earthq. Eng. Struct. Dyn., 7(3): 253-263, 1979.

[8] Ministry of Land, Infrastructure, Transport and Tourism, Japan 2000, “Notification 1461”, A notification of Japanese regularization for seismic design.

[9] K. K. Krishnamoorthy and T. Mathew, Statistical tolerance regions: theory, applications, and computation. Wiley, 2009.

[10] P. B. Schnabel, J. Lysmer and H.B. Seed, “SHAKE a computer program for earthquake response analysis of horizontally layered sites”, ERRC, 72-12, 1972.

[11] B. O. Hardin and V. P. Drnevich, Shear Modulus and Curves. ASCE, Vol.98, No.SM7, 667-692, 1972.

[12] F. McKenna, OpenSees: A framework for earthquake engineering simulation. Comput. Sci. Eng., 13(4): 58-66, 2011.